



OPEN Time evolution of piglet cerebral blood volume after resuscitation from hypoxic-ischemic insult

Manabu Machida¹✉, Tsutomu Mitsue², Yasuhiro Nakao³, Yinmon Htun³, Aya Morimoto⁴, Uiko Hanaoka⁵, Yukihiko Konishi⁶, Kosuke Koyano⁴, Shinji Nakamura³ & Takashi Kusaka³

Neonatal hypoxic-ischemic encephalopathy (HIE) is a significant cause of neonatal mortality and developmental disabilities. It has been revealed that the temporal behavior of the cerebral blood volume (CBV) carries information on the degree of hypoxia-ischemia. CBV can be estimated by means of near-infrared spectroscopy. The change of CBV after the insult is related to the change of CBV during the insult. In this paper, we consider a mathematical model which governs the time evolution of CBV after the insult. We show that the temporal behavior of CBV can be predicted with the Kalman filter which is based on the mathematical model. Finding a governing equation opens up possibilities for a more quantitative diagnosis of HIE.

Neonatal hypoxic-ischemic encephalopathy (HIE) causes death and developmental disabilities in newborns¹. It occurs in about 2-3 per 1000 births in developed countries^{2,3}. It is primarily caused by a lack of oxygen and blood flow to the brain due to factors such as birth asphyxia, maternal conditions, and placental insufficiency. Understanding HIE requires evaluating changes in cerebral circulation and oxygen metabolism to develop effective interventions. It is essential to initiate therapeutic hypothermia early (within six hours after birth but earlier is better) to improve survival and neurodevelopmental outcomes for asphyxiated neonates with moderate-to-severe HIE^{4,5}.

Since near-infrared light is particularly absorbed by hemoglobin, cerebral blood volume (CBV) can be estimated with near-infrared spectroscopy (NIRS) using the time-resolved spectroscopy (TRS, Hamamatsu Photonics K.K.). For the piglet experiment which will be considered in this paper, two optical fibers (one is for emission and the other is for detection) were attached to the head of each piglet with the source-detector distance 30 mm (the typical penetration depth is about a centimeter). In TRS, the time-correlated single-photon counting technique is used to detect photons. By photon detection with three wavelengths, the oxyHb and deoxyHb concentrations can be estimated, which can then be converted to CBV^{6,7}. TRS has a non-invasive technique for continuous monitoring that allows repeated NIRS measurements to create a time series of measured data. The use of NIRS for monitoring cerebral hemodynamics and oxygenation has provided useful insights for the management of newborns^{8,9}. By conducting a retrospective study of 11 neonates admitted to the NICU at Kagawa University, it was indicated that the change of CBV was more prominently related to the clinical outcome than the change of cerebral hemoglobin oxygen saturation (S_cO_2)¹⁰.

Previously, we reported how CBV during and after HI insult changed and that CBV after insult reflected histopathological brain injuries in piglet¹¹⁻¹⁴. In piglets subjected to the HI insult, CBV initially rises to a peak and then keeps decreasing until resuscitation. After resuscitation, a piglet with more reduction during insult shows more increase after insult. Hence, these changes in the CBV pattern are related to the severity of brain injuries caused by autoregulatory impairment. Impaired cerebral autoregulation results in adverse neurological outcomes^{15,16}. The time evolution of CBV reflects the degree of hypoxia-ischemia. In particular, the dependence of the temporal change γ after the insult on the decay amount x of CBV during the HI insult was investigated¹³.

In this paper, we focus on the temporal change of CBV for HIE experiments with piglets. To predict the time evolution of CBV after the insult, it is desirable to find a differential equation which governs the phenomenon. This situation is somewhat similar to weather forecast, which is based on the primitive equations. The change of CBV in time takes place as a consequence of extremely complicated blood flows in the body, which in principle

¹Department of Informatics, Faculty of Engineering, Kindai University, Hiroshima, Japan. ²Medical Engineering Equipment Management Center, Kagawa University Hospital, Kagawa, Japan. ³Department of Pediatrics, Faculty of Medicine, Kagawa University, Kagawa, Japan. ⁴Maternal Perinatal Center, Kagawa University, Kagawa, Japan. ⁵Department of Perinatology and Gynecology, Faculty of Medicine, Kagawa University, Kagawa, Japan. ⁶Department of Education for Children with Special Needs, Kagawa University, Kagawa, Japan. ✉email: machida@hiro.kindai.ac.jp

can be described by the fluid dynamics. Without touching detailed blood flows in the head, we seek a differential equation which is able to reproduce the time evolution of CBV. This is in some sense related to seeking laws of thermodynamics without statistical mechanics. In this paper, we propose a differential equation which governs the time evolution of CBV for the piglets. To validate the mathematical model, we predict the time dependence of CBV using the observed data from the piglet experiments. The Kalman filter was used for the prediction.

The Kalman filter is a technique to correct the time evolution obtained by a mathematical model using observation. Suppose that a wave moves with a constant velocity. The waveform obeys the transport equation with the first-order space and time derivatives. Even though we know that the wave moves from left to right, the mathematical model may not be exact due to the uncertainty about the wave speed and whether the linear wave propagation model is correct. To compensate for the difference between the ideal and actual situations, the prediction by the governing equation need to be modified using measurement data (see, for example, the textbook by Kaipio and Somersalo¹⁷).

The Kalman filter, including the extended Kalman filter, has been used for a pulmonary blood flow estimator¹⁸, cerebral blood flow autoregulation^{19,20}, and the heart rate detection with reflected light²¹, microvessel imaging for microvessel density maps and blood flow speed maps²², and the hemodynamic responses for functional near-infrared spectroscopy²³. See a review by Nolte and Bertoglio for the blood flow for the cardiovascular system²⁴.

Since it is not easy to obtain the time dependence of CBV for neonates and even newborn piglets, the Kalman filter has not been used in the context of neonatal HIE. Moreover, to the best of our knowledge, any mathematical model has not been proposed for the time evolution of CBV for the neonatal HIE.

Results

Figure 1 shows the temporal change y (mL per 100 g) of CBV beginning at the resuscitation from the HI insult for different x (mL per 100 g), which is the difference of the blood volume between the maximum value during the insult and the value at the beginning of the resuscitation. See Ref. ¹³ for piglet experiments for the data shown in Fig. 1. Measurements were performed every 10 sec and averages of six measurements were taken to plot the temporal profile every minute. In Fig. 1, the red line with solid circles is y for $x = 1.85$, the other line with open squares is y for $x = 1.324$, and the green line with diagonal crosses is y for $x = 0.993$.

For each curve in Fig. 1, one-step prediction was done with the Kalman filter. Curves in Fig. 1 are drawn with $N + 1$ points (t_i, y_i) ($i = 0, 1, \dots, N$). Here, $N = 20$. We note that $t_i - t_{i-1} = 1$ min ($i = 1, \dots, N$). In each of three panels of Fig. 2, predicted values of y_i were computed with the Kalman filter using y_1, \dots, y_{i-1} . The linear mathematical model (see below) was used for the Kalman filter. In this way, the actual values (red) and predicted values (blue) are compared in each panel. In the panels of Fig. 2, green points show the standard deviation of the error at each time. In the case of $x = 0.993$, $\omega = 0.446$ rad/min. In the case of $x = 1.324$, $\omega = 0.370$ rad/min. In the case of $x = 1.85$, $\omega = 0.243$ rad/min. In all cases, $t_c = 1$ min, $x_p = 1.5$, $a = 1$, $b = 0.3$. The unit of time was hour instead of minute for the Kalman filter, in which case $\Delta\tau = 1/60$ hr.

In Figs. 3 and 4, prediction for longer times was considered. Figure 3 shows an example of y which decays in time and Fig. 4 shows an example of y which grows in time. In the top left panels of Figs. 3 and 4, predicted values are plotted for the last 5 min. That is, the Kalman filter algorithm did not use observed data for the last 5 min. Similarly, in the top right panels of Figs. 3 and 4, predicted values for the last 10 min are plotted. In the bottom panels of Figs. 3 and 4, predicted values for the last 15 min are plotted.

The parameters in the proposed mathematical model were chosen to reproduce the observed behavior of y . In particular, the same β, b were used for Figs. 2, 3, and 4. Figure 5 illustrates predicted values when other β, b are used.

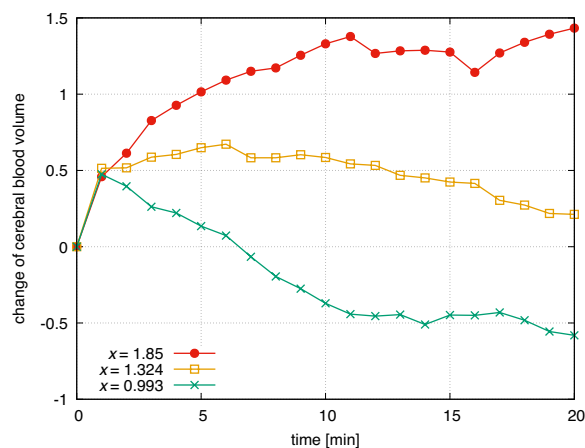


Fig. 1. Time evolutions of the change y of CBV for three cases which are used in this paper. Here, x denotes the change of CBV during the insult. From the top, the red line is for $x = 1.85$, other line is for $x = 1.324$, and green line is for $x = 0.993$.

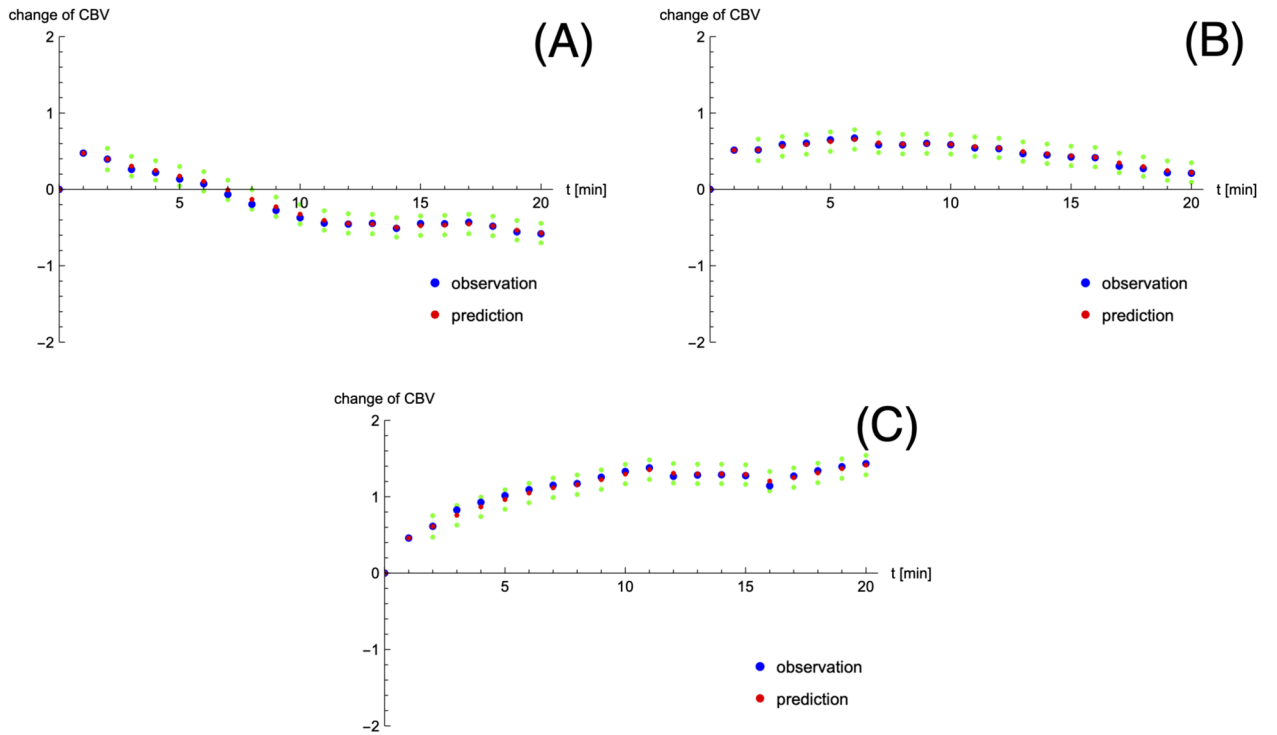


Fig. 2. One-step (1 min) predictions for (A) $x = 0.993, \omega = 0.446$, (B) $x = 1.324, \omega = 0.370$, and (C) $x = 1.85, \omega = 0.243$. Blue circles show the observed data and red circles mean predicted values. Moreover, green circles show the standard deviation of the estimated error in upper and lower directions.

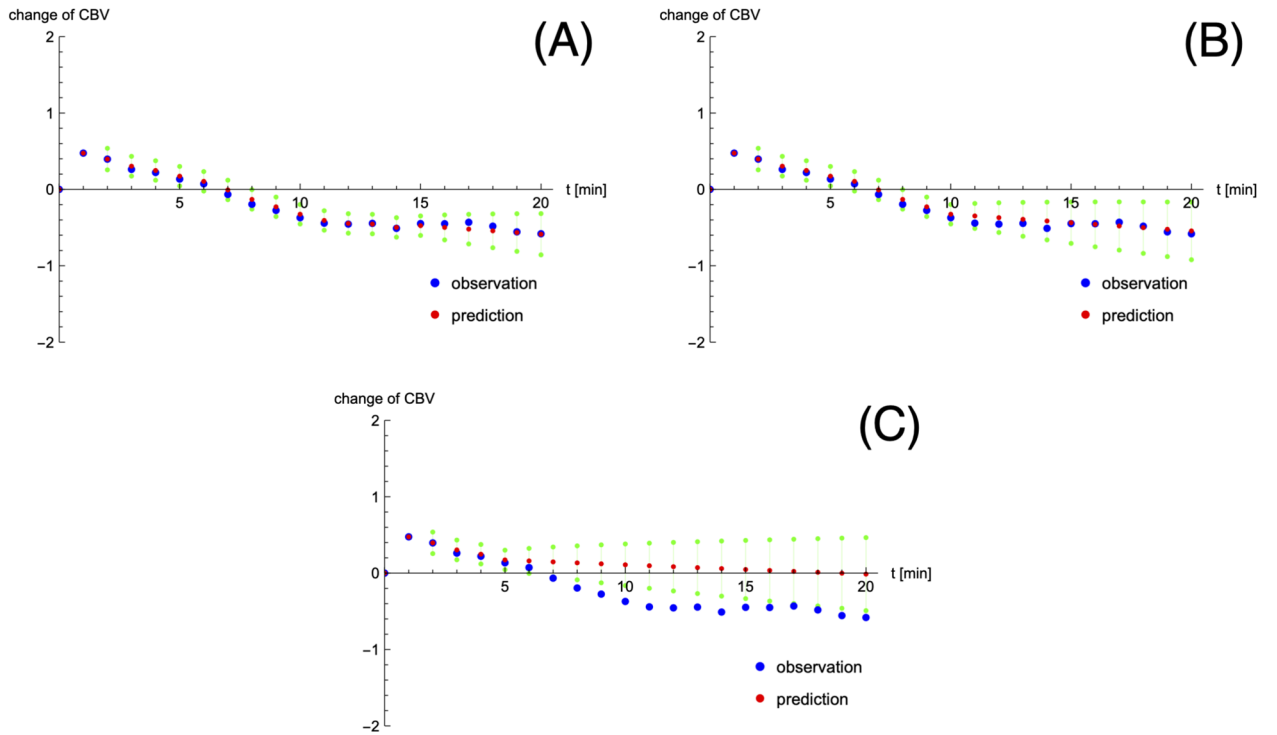


Fig. 3. Predictions for the last (A) 5 min, (B) 10 min, and (C) 15 min in the case of $x = 0.993, \omega = 0.446$.

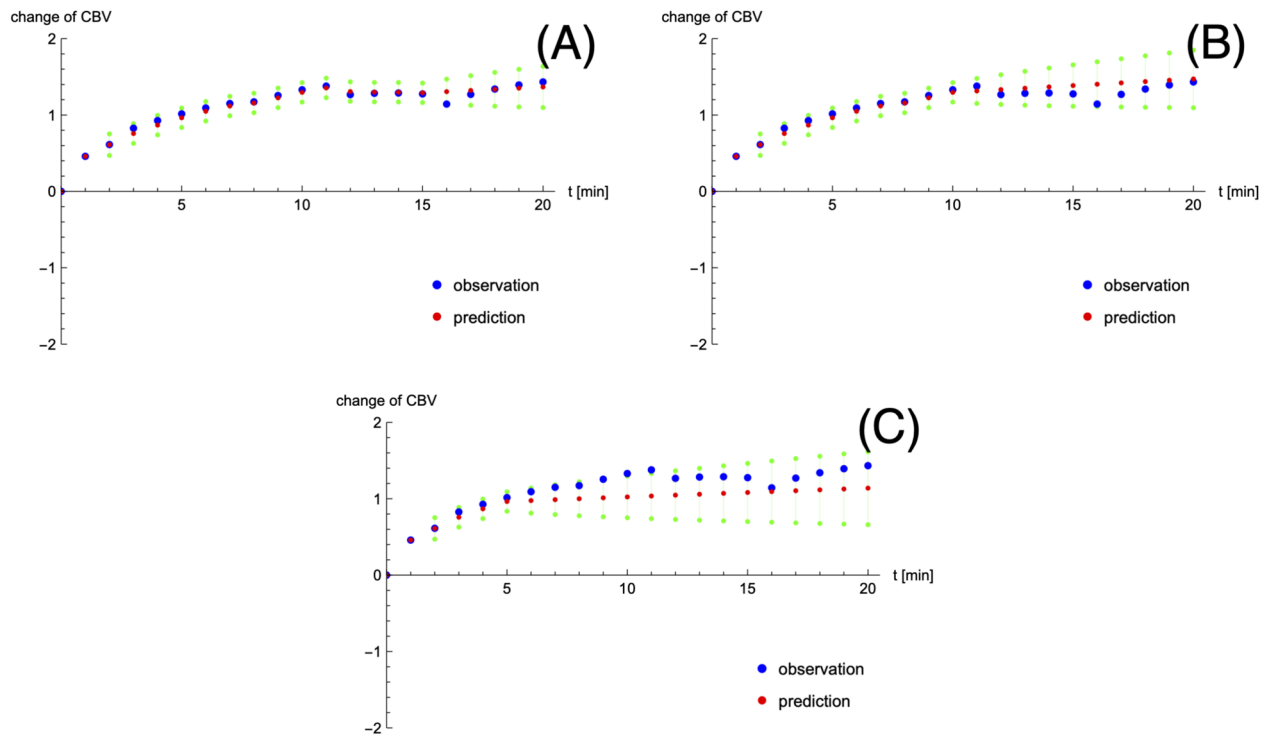


Fig. 4. Predictions for the last (A) 5 min, (B) 10 min, and (C) 15 min in the case of $x = 1.85$, $\omega = 0.243$.

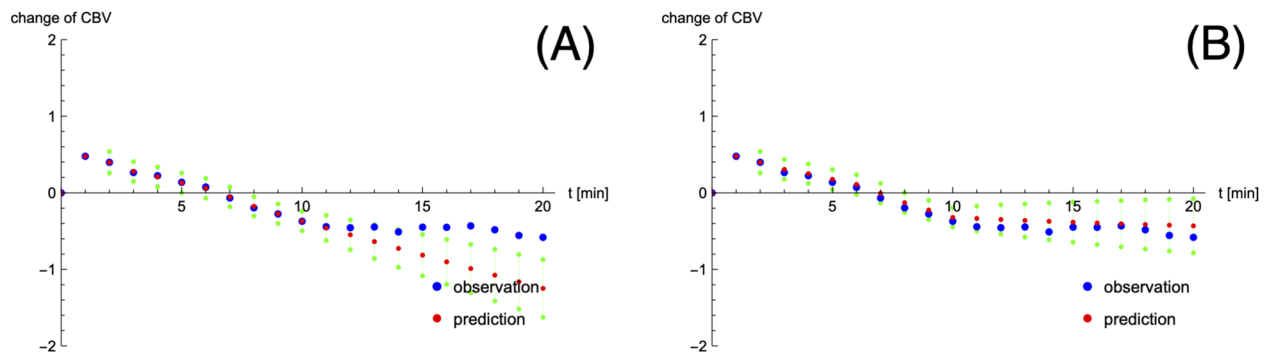


Fig. 5. These graphs correspond to the top right panel of Fig. 3. In the case of $x = 0.993$, (A) $a = 10$ and (B) $b = 3$ while other parameters are the same as the parameters used in Fig. 3.

Discussion

As shown in Fig. 1, the change y of CBV has an increasing tendency, a decreasing tendency, or no strong increasing nor decreasing behavior. The major cause of such variety is the amount x of the drop of CBV during the HI insult between the peak time and the resuscitation time¹³. During the HI insult, CBV initially rises rapidly as a compensatory response, followed by impaired cerebral blood flow autoregulation and vasoparalysis, leading to a gradual decrease in CBV as decompensation sets in. It was found that a large decrease of CBV from the baseline during insult was associated with severe brain injury or mortality¹¹.

Since the change of y during 1 min is monotonic, the one-step prediction (prediction every minute) worked well as shown in Fig. 2. In Fig. 2, predicted values agree with the observed data after the first a few minutes of the filtering process of the Kalman filter.

Longer predictions were performed in Figs. 3 and 4. We can observe that predictions within 10 min work quite well. Since longer predictions were tested using the same time-series data up to 20 min, the filter process becomes shorter for longer prediction. Moreover, since the linear model is used for the Kalman filter, it is not possible to predict nonmonotonic behavior of CBV.

We properly chose parameters in the mathematical model. This is explained in Fig. 5. The prediction is not successful if other parameters are chosen. We emphasize that the parameter x , ω depend on individual sample but otherwise the same parameters were used for all samples in Figs. 2 through 4.

In principle, parameters in the mathematical model depend on factors such as blood pressure and heart rate, as well as sex difference, presence or absence of infections, and severity. For example, it was observed for both piglets¹³ and fetal sheep²⁵ that if the heart rate increases more during insult, it also increases more after the insult.

We note that CBV in the brain is not homogeneous²⁶. Moreover, since the TRS assumes a homogeneous half-space domain when it estimates absorption and scattering coefficients using the diffusion theory, the estimated CBV by TRS deviates from the true value of the blood volume. However, our previous studies showed that the change of this CBV is related to the degree of HIE (see Mitsui, et al., Scientific Reports (2021)¹³ and references therein). Hence, in this paper, we seek a mathematical model for this CBV.

CBV obtained with TRS primarily reflects hemodynamics in the superficial cerebral cortex. However, neonates have small heads and only a short distance separates the cortex from the subcortical white matter. Hence, ischemic changes are likely to develop in both layers simultaneously. Particularly in HIE, ischemic injuries of the subcortical white matter and deep gray matter often coexist²⁷. Changes in the superficial cortex detected by TRS may indirectly reflect metabolic disorders in deeper areas of the brain.

It should be emphasized that the proposed mathematical model describes the change of CBV due to the hypoxic–ischemic insult. Hence the model is phenomenological. The hepatic portal vein flow was simulated using the Navier–Stokes equation with a fractal tree network²⁹. The mathematical modeling of solutes absorption processes by the arterial wall was discussed³⁰. The blood flow in the capillary network on a tumor was simulated³¹. Unlike these above studies, the relation between the dynamics of CBV due to HIE and differential equations is an open problem and no mathematical model had been known. Although during the first 20 min after birth, we could move the situation one step forward with the proposed mathematical model.

Conclusion

In this paper, we explored the change of CBV during 20 minutes after the HI insult in neonatal piglets with HIE. In general, a large CBV decrease during the insult causes an increase of the post-insult CBV.

We proposed a mathematical model which can reproduce the behavior that greater decreases in CBV during the HI insult are followed by more pronounced increases after the insult.

Based on the proposed linear model, we showed that the time evolution of CBV can be predicted with the Kalman filter. This fact implies that the proposed model governs the change of CBV in time for neonatal HIE.

Materials and methods

Model

Let $V(t)$ be the cerebral blood volume [mL] (per 100 g) at time t [hr]. We suppose that the hypoxic-ischemic period ends at $t = 0$. Let $t_{\max} > 0$ be the maximum time ($t_{\max} = 1/3$ in this paper). Since y is the change of CBV after the insult, CBV at time t can be calculated as the sum of CBV at the beginning of the resuscitation and y . We can express $V(t)$ as

$$V(t) = v_{\max} - x + y(t; x), \quad 0 < t < t_{\max},$$

where x is the blood volume which goes away from the brain after it reaches the peak v_{\max} until $t = 0$ and $y(t; x)$ is the change of the cerebral blood volume for $t > 0$.

Our previous research with piglets implied that $y(t; x)$ rotates about the origin of the x - y plain for small $t > 0$ and then starts rotating about another point (x_p, y_p) ¹³. In light of this observation, we make the following model:

$$y(t; x) = \begin{cases} x \tan(\omega t), & 0 < t \leq t_c, \\ u(\tau; x) + y(t_c; x), & \tau = t - t_c, \quad t_c < t < t_{\max}, \end{cases} \quad (1)$$

where ω is a positive constant. Here, we supposed that $y(t; x)$ rotates about the origin in the x - y plane until time t_c . We note that the angular frequency ω is given by

$$\omega = \frac{1}{t_c} \tan^{-1} \left(\frac{y_p}{x_p} \right).$$

Thus, ω can be determined if x_p, y_p, t_c are estimated from observed data. For later use let us introduce the distance $\xi(x)$ in the x - y plane between a point (x, y) and (x_p, y_p) at time t_c , which is expressed as

$$\xi(x) = \frac{x - x_p}{\cos(\omega t_c)}.$$

Next, we consider $u(\tau; x)$. By looking at the temporal behavior of points in the x - y plane, where each point corresponds to one experiment with a piglet¹³, we regard u as the position of a particle that moves according to Newton's equation of motion. Since the motion is the change of CBV, the particle should stop eventually. This time-evolution can be achieved by the introduction of a friction term. Let us consider the equation of motion in the presence of friction:

$$\frac{d^2 u}{d\tau^2} = -b \frac{du}{d\tau}, \quad b > 0. \quad (2)$$

We give the initial conditions as

$$u(0) = 0, \quad \frac{du}{d\tau}(0) = a\xi(x),$$

where a is a positive constant. Since the initial velocity is proportional to ξ , the initial speed is slow is the point $(x, y(t_c; x))$ is close to (x_p, y_p) . The mathematical model which is given in (1) and (2) is simple but satisfies observed temporal behavior of the experimental data.

The solution to (2) is obtained as

$$u(\tau) = \frac{a}{b}\xi(x) (1 - e^{-b\tau}).$$

The Kalman filter

Let us discretize time to apply the Kalman. We have

$$\begin{cases} \frac{d}{d\tau} \begin{pmatrix} u \\ v \end{pmatrix} = \begin{pmatrix} v \\ -bv \end{pmatrix}, & \tau > 0, \\ \begin{pmatrix} u(0) \\ v(0) \end{pmatrix} = \begin{pmatrix} 0 \\ a\xi(x) \end{pmatrix}. \end{cases}$$

Let us discretize time as $t_k = k\Delta\tau$ ($t_c = k_c\Delta\tau$). We can write

$$\begin{pmatrix} u_k \\ v_k \end{pmatrix} = \begin{pmatrix} u_{k-1} + v_{k-1}\Delta\tau \\ v_{k-1} - bv_{k-1}\Delta\tau \end{pmatrix}$$

for $k = k_c + 1, \dots$. Let us set

$$F = \begin{pmatrix} 1 & \Delta\tau \\ 0 & 1 - b\Delta\tau \end{pmatrix}, \quad H = (1 \quad 0).$$

The state equation and observation equation are given by

$$x_k = Fx_{k-1} + w^{(1)}, \quad y_k(x) = Hx_k + w^{(2)},$$

where $w^{(1)} \in \mathbb{R}^2$ and $w^{(2)} \in \mathbb{R}$ are Gaussian noise for the system and measurement noise. Let Q, R be diagonal system noise and measurement error covariance matrices:

$$Q = E [w^{(1)}w^{(1)T}] \in \mathbb{R}^2, \quad R = E [w^{(2)2}] \in \mathbb{R},$$

where $E[\cdot]$ denotes the expectation value. We set $Q = 0.01I, R = 0.01$, where I is the 2×2 identity matrix.

Let \hat{x}_k be the estimated state vector. The calculation consists of the prediction and update steps²⁸. The prediction step is done as follows. We have

$$\mathbb{R}^2 \ni \hat{x}_{k|k-1} = F\hat{x}_{k-1}, \quad \mathbb{R}^{2 \times 2} \ni P_{k|k-1} = FP_{k-1}F^T + Q.$$

Here, the error covariance matrix P_k is given by

$$P_k = E [(x_k - \hat{x}_k)(x_k - \hat{x}_k)^T].$$

Initially we set $P_{k_c} = I$. Then the update step is performed as follows:

$$\begin{aligned} \mathbb{R} \ni z_k &= y_k - H\hat{x}_{k|k-1}, \\ \mathbb{R} \ni S_k &= HP_{k|k-1}H^T + R = \{P_{k|k-1}\}_{11} + R, \\ \mathbb{R}^2 \ni K_k &= P_{k|k-1}H^T S_k^{-1} = \begin{pmatrix} \{P_{k|k-1}\}_{11} \\ \{P_{k|k-1}\}_{21} \end{pmatrix} \frac{1}{S_k}, \\ \mathbb{R}^2 \ni \hat{x}_k &= \hat{x}_{k|k-1} + K_k z_k, \\ \mathbb{R}^{2 \times 2} \ni P_k &= (I - K_k H) P_{k|k-1}. \end{aligned}$$

Let us consider the j -step prediction. After $k = k_M$, we have

$$\begin{aligned} \hat{x}_{k_M+i} &= F\hat{x}_{k_M+i-1}, \\ P_{k_M+i} &= FP_{k_M+i-1}F^T + Q \end{aligned}$$

for $i = 1, \dots, j$.

Data availability

The data that support the findings of this study are available from the corresponding author upon reasonable request.

Received: 11 March 2025; Accepted: 14 July 2025

Published online: 23 July 2025

References

- Merchant, N. & Azzopardi, D. Hypoxic ischaemic encephalopathy in newborn infants. *Fetal Matern. Med. Rev.* **21**, 242–262 (2010).
- Evans, K., Rigby, A. S., Hamilton, P., Titchiner, N. & Hall, D. M. The relationships between neonatal encephalopathy and cerebral palsy: a cohort study. *J. Obstet. Gynaecol.* **21**, 114–120 (2001).
- Law, J. E., Wilczynska-Ketende, K. & Cousens, S. N. Estimating the causes of 4 million neonatal deaths in the year 2000. *Int. J. Epidemiol.* **35**, 706–718 (2006).
- Thoresen, M. et al. Time is brain: Starting therapeutic hypothermia within three Hours after birth improves motor outcome in asphyxiated newborns. *Neonatology* **104**, 228–233 (2013).
- Davidson, J. O., Wassink, G., van den Heuij, L. G., Bennet, L. & Gunn, A. J. Therapeutic hypothermia for neonatal hypoxic-ischemic encephalopathy - where to from here?. *Front. Neurol.* **6**, 198 (2015).
- Ijichi, S. et al. Quantification of cerebral hemoglobin as a function of oxygenation using near-infrared time-resolved spectroscopy in a piglet model of hypoxia. *J. Biomed. Opt.* **10**, 024026 (2005).
- Ijichi, S. et al. Developmental changes of optical properties in neonates determined by near-infrared time-resolved spectroscopy. *Pediatr. Res.* **58**, 568–573 (2005).
- Dix, L. M., van Bel, F. & Lemmers, P. M. Monitoring cerebral oxygenation in neonates: an update. *Front. Pediatr.* **5**, 46 (2017).
- Kusaka, T. et al. Evaluation of cerebral circulation and oxygen metabolism in infants using near-infrared light. *Brain Dev.* **36**, 277–283 (2014).
- Nakamura, S. et al. Simultaneous measurement of cerebral hemoglobin oxygen saturation and blood volume in asphyxiated neonates by near-infrared time-resolved spectroscopy. *Brain Dev.* **37**, 925–932 (2015).
- Nakamura, S. et al. Cerebral blood volume combined with amplitude-integrated EEG can be a suitable guide to control hypoxic/ischemic insult in a piglet model. *Brain Dev.* **35**, 614–625 (2013).
- Nakamura, M. et al. Cerebral blood volume measurement using near-infrared time-resolved spectroscopy and histopathological evaluation after hypoxic-ischemic insult in newborn piglets. *Int. J. Dev. Neurosci.* **42**, 1–9 (2015).
- Mitsuie, T. et al. Cerebral blood volume increment after resuscitation measured by near-infrared time-resolved spectroscopy can estimate degree of hypoxic-ischemic insult in newborn piglets. *Sci. Rep.* **11**, 13096 (2021).
- Nakao, Y. et al. Cerebral hemodynamic response during the resuscitation period after hypoxic-ischemic insult predicts brain injury on day 5 after insult in newborn piglets. *Sci. Rep.* **12**, 13157 (2022).
- Ferriero, D. M. Neonatal brain injury. *N. Engl. J. Med.* **351**, 1985–1995 (2004).
- Alderliesten, T., Lemmers, P. M. A., Smarius, J. J. M., van de Vosse, R. E., Baerts, W. van Bel, F. Cerebral oxygenation, extraction, and autoregulation in very preterm infants who develop peri-intraventricular hemorrhage. *J. Pediatr.* **162**, 698–704, e2 (2013).
- Kaipio, J. P. *Somersalo* (Springer, E. Statistical and Computational Inverse Problems, 2005).
- Brovko, O., Wiberg, D. M., Arena, L. & Bellville, J. W. The extended Kalman filter as a pulmonary blood flow estimator. *Automatica* **17**, 213–220 (1981).
- Masnadi-Shirazi, M. A., Behbehani, K., Zhang, R. Kalman filter modeling of cerebral blood flow autoregulation. *The 26th Annual International Conference of the IEEE Engineering in Medicine and Biology Society*, 734–737 (2004).
- Aoi, M., Gremaud, P., Tran, H. T., Novak, V., Olufsen, M. S. Modeling cerebral blood flow and regulation. *31st Annual International Conference of the IEEE EMBS Minneapolis, Minnesota, USA, September 2–6*, 5470–5473 (2009).
- Kumar, S., Prakash, A. & Tucker, C. S. Bounded Kalman filter method for motion-robust, non-contact heart rate estimation. *Biomed. Opt. Express* **9**, 873–897 (2018).
- Tang, S. et al. Kalman filter-based microbubble tracking for robust super-resolution ultrasound microvessel imaging. *IEEE Trans. Ultrason. Ferroelectr. Freq. Control.* **67**, 1738–1751 (2020).
- Dong, S. & Jeong, J. Improvement in recovery of hemodynamic responses by extended Kalman filter with non-linear state-space model and short separation measurement. *IEEE Trans. Biomed. Eng.* **66**, 2152–2162 (2019).
- Nolte, D. & Bertoglio, C. Inverse problems in blood flow modeling: A review. *Int. J. Numer. Method Biomed. Eng.* **38**, e3613 (2022).
- Yamaguchi, K. et al. Evolving changes in fetal heart rate variability and brain injury after hypoxia-ischaemia in preterm fetal sheep. *J. Physiol.* **596**, 6093–6104 (2018).
- Wintermark, P., Moessinger, A. C., Gudinchet, F. & Meuli, R. Perfusion-weighted magnetic resonance imaging patterns of hypoxic-ischemic encephalopathy in term neonates. *J. Mag. Res. Imaging* **28**, 1019–1025 (2008).
- Weeke, L. C. et al. A novel magnetic resonance imaging score predicts neurodevelopmental outcome after perinatal asphyxia and therapeutic hypothermia. *J. Pediatr.* **192**, 33–40, e2 (2018).
- Simon, D. *Optimal State Estimation*, John Wiley Sons, (2006).
- Xie, C. et al. Numerical prediction of portal hypertension by a hydrodynamic blood flow model combining with the fractal theory. *J. Biomechanics* **150**, 111504 (2023).
- Quarteroni, A., Veneziani, A. & Zunino, P. Mathematical and numerical modeling of solute dynamics in blood flow and arterial walls. *SIAM J. Numerical Analysis* **39**, 1488–1511 (2002).
- Soltani, M. & Chen, P. Numerical modeling of interstitial fluid flow coupled with blood flow through a remodeled solid tumor microvascular network. *PLoS ONE* **8**, e67025 (2013).

Author contributions

M.M. designed the study and drafted the article. T.M., S.N., and T.K. performed the animal experiments. M.M. performed the data analysis. T.M., Y.N., Y.H., A.M., U.H., Y.K., K.K., S.N., and T.K. contributed to the interpretation of the data. All authors critically revised the manuscript and contributed to the final approval of the version to be published.

Funding

This work was supported by JST, PRESTO Grant Number JPMJPR2027. This study was also financially supported by JSPS KAKENHI Grants-in-Aid (Nos. 23K07292, 23K07332, 22K07822, 22K15922, 22K15923, 22K18171); Kagawa University Faculty of Medicine School of Medicine Alumni Association Sanjukai Research Aid (R5-1).

Declarations

Competing interests

The authors declare no competing interests.

Additional information

Correspondence and requests for materials should be addressed to M.M.

Reprints and permissions information is available at www.nature.com/reprints.

Publisher's note Springer Nature remains neutral with regard to jurisdictional claims in published maps and institutional affiliations.

Open Access This article is licensed under a Creative Commons Attribution-NonCommercial-NoDerivatives 4.0 International License, which permits any non-commercial use, sharing, distribution and reproduction in any medium or format, as long as you give appropriate credit to the original author(s) and the source, provide a link to the Creative Commons licence, and indicate if you modified the licensed material. You do not have permission under this licence to share adapted material derived from this article or parts of it. The images or other third party material in this article are included in the article's Creative Commons licence, unless indicated otherwise in a credit line to the material. If material is not included in the article's Creative Commons licence and your intended use is not permitted by statutory regulation or exceeds the permitted use, you will need to obtain permission directly from the copyright holder. To view a copy of this licence, visit <http://creativecommons.org/licenses/by-nc-nd/4.0/>.

© The Author(s) 2025